Chapter 1
Fundamentals of Noise in Optoelectronics

Peter Seitz

Abstract Electromagnetic radiation can be described as a stream of individual photons. In solid-state detectors (e.g., photocathodes or semiconductor photosensors), each photon of sufficient energy creates one or several mobile charge carriers which can be subsequently detected with sensitive electronic circuits, possibly after charge packet multiplication employing the avalanche effect. Two types of noise limit the resolution with which individual photons can be detected: (1) The number of detectable photons or photoelectrons shows a statistical variation, which is often well-described as a Poisson distribution. (2) Photogeneration of mobile charge carriers competes with thermal generation, and thermal noise is compromising the generation of photocharges ("dark current") as well as the performance of electronic charge detection circuits ("Johnson noise" and "random telegraph signal noise"). It is shown that the laws of physics and the performance of today's semiconductor fabrication processes allow the detection of individual photons and photocharges in image sensors at room temperature and at video rate.

1.1 Introduction

At the end of the nineteenth century, it was realized that the classical description of light as an electromagnetic wave satisfying Maxwell's equation fails to properly explain important optical phenomena. In particular, the interaction with matter, such as the emission or absorption of light, requires an improved theoretical framework. The breakthrough came with Einstein's hypothesis that light consists of quanta of energy [1], the so-called photons. As a consequence, the measurement of properties of electromagnetic radiation has an ultimate limit, imposed by the description of light as a stream of individual photons. It is only natural, therefore, that scientists and engineers alike want to perform their measurements of light to this ultimate precision, the single photon.

As we will work out in this contribution, the main obstruction to achieving this goal is, ironically, the presence of electromagnetic radiation. This is, of course, the ubiquitous blackbody radiation surrounding us whenever the temperature of our environment is not identical to zero. The goal of the present work is to understand how the coupling between this omnipresent "temperature bath" and matter influences our measurements of light, elucidating under which circumstances single-photon sensing of light is possible in practice.

In a first part, basic properties of quantized systems are recalled, in particular essential properties of the Poisson distribution. In the second part, the noise properties of most common light sources are investigated, revealing that under most practical conditions, the photons of these light sources have essentially a Poisson distribution. In the third part, the energy band model of solid state matter is employed to explain the principles and fundamental limitations of photosensing with semiconductors. In the fourth part, noise sources in relevant electronic components and circuits are studied, to determine the ultimate, temperature-dependent limits of the electronic detection of charge. Finally, all the material is brought together for a concise summary of the physical and technological limits of the detection of light, explaining under which circumstances single-photon imaging is possible.

1.2   Quantization of Electromagnetic Radiation, Electrical Charge, and Energy States in Bound Systems

The photoelectric effect – the emission of electrons from solid matter as a result of the absorption of energy from electromagnetic radiation – seems to be compelling evidence for the existence of photons. Actually, this is not the case: Although it is true that the atoms in solid matter are absorbing energy from a light beam in quantized packets, this can also be understood in a semiclassical picture in which light is described as a classical electromagnetic wave and only the atoms are treated as quantized objects [2]. Careful analysis along similar lines can also show that the individual pulses detected with "single-photon counting devices" are not conclusive evidence for the existence of photons.

It is an astonishing fact that there are only relatively few optical phenomena that cannot be explained with a semiclassical theory [2]. Of course, only the full quantum optical approach in the framework of quantum electrodynamics (QED) is completely consistent, both with itself and with the complete body of experimental evidence [3]. QED mathematically describes the interaction between light and matter by specifying how electrically charged particles interact through the exchange of photons.

Despite this surprising fact that the photon concept is not really required to understand photodetectors, the simplicity, intuitiveness and basic correctness of the corpuscular photon picture makes it so attractive that it is adopted by most researchers in the field.

As a consequence, we consider light to be a stream of photons, individual particles of zero rest mass traveling at the speed of light $c = 2.9979 \times 10^8$ m/s in vacuum and at retarded speeds in matter. The wavelike nature of the photon is reflected in the fact that a frequency ν and a corresponding wavelength λ can be associated with it, so that the energy E of a photon is given by:

$$E = h\nu = \frac{hc}{\lambda} \tag{1.1}$$

with Planck's constant $h = 6.6262 \times 10^{-34}$ Js.

Each atom of matter consists of a system of several electrons bound to the protons in a nucleus by the attractive Coulomb force. The electron is a subatomic elementary particle carrying a negative charge of $-q$, with the unit charge $q = 1.6022 \times 10^{-19}$ C. In effect, the electrical charge of any particle is always found to be a multiple of this unit charge, making electrical charge also a quantized physical property.

Finally, according to quantum mechanics, the bound system of an atom does not have stable states with arbitrary energies. Rather, only a discrete set of stable states, each with its proper energy level, is allowed [4]. It is concluded that also the energy states of a bound system are quantized.

1.3 Basic Properties of the Poisson Distribution

In any kind of counting problem, the Poisson distribution arises as an almost inevitable consequence of statistical independence [5]. For this reason, the Poisson distribution is clearly the most important probability law in photon or electron counting problems. The typical question asked in such a problem is the following: What is the probability $p_N(k)$ that a number $k \geq 0$ of events is observed during a fixed observation period T if these events occur with a known average rate N/T and, independent of the time since the last event? The quantity N describes, therefore, the average number of events observed during the time T. The sought probability distribution $p_N(k)$ is the Poissonian:

$$p_N(k) = \frac{N^k e^{-N}}{k!}. \tag{1.2}$$

In Fig. 1.1 the Poisson distributions for the three small expectation values $N = 1$, $N = 4$, and $N = 9$ are depicted.

The Poisson distribution has a few surprising properties, for example the fact that if the average number of observed events is $N = 1$, the probability that no events are observed ($k = 0$) is the same as the probability that exactly one event occurs ($k = 1$). And because $p_1(1) = 0.368$, we observe exactly one event only in about a third of the cases.

Another important property of the Poisson distribution is its relation to Bernoulli trials. A Bernoulli trial is an experiment whose outcome is random and can only
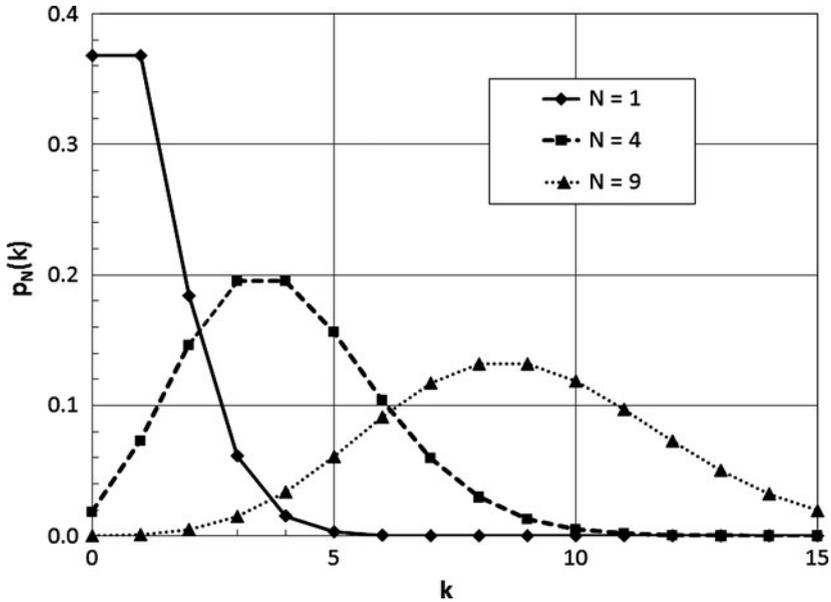
Fig. 1.1 Poisson distribution $p_N(k)$ for three different cases of small expectation value N. These are discrete distributions, and the connecting lines serve only as visual aids

be of two possible outcomes, either "success" or "failure." If consecutive Bernoulli trials, a sequence which is called "binomial selection," are statistically independent of each other with a fixed success probability η, the so-called *binomial selection theorem* holds [5]:

Binomial selection of a Poisson process yields a Poisson process, and the mean M of the output of the selection process is the mean N of the input times the success probability η, $M = \eta \cdot N$.

The complete physical process of the detection of photons can be described mathematically as a cascade of binomial selection processes. If we can assure that the input to this whole chain of events is a Poisson process then we are certain that the output of the whole detection process is also a Poisson process. In Sect. 1.4 the different types of interaction processes between electromagnetic radiation and matter are investigated, leading to the insight that all these processes are, indeed, cascades of binomial selection processes. In Sect. 1.5, the photon emission properties of the most common light sources are examined, and under many practical conditions, the emitted photon streams shows, indeed, a Poisson distribution.

As a consequence, the probabilistic description of the photodetection process becomes very simple in most practical cases: Wherever in an experiment one samples and inspects photon streams or photogenerated charges, they are Poisson distributed!

1.4   Interaction of Radiation and Matter

The actual detection of electromagnetic radiation is a complicated process, involving many types of interactions between light and matter, such as reflection, refraction, diffraction, scattering, absorption, and electronic conversion. Each of these individual processes, however, is by itself a binomial selection process or a sequence of binomial selection processes.

As illustrated in Fig. 1.2, the most common interactions between light and matter include the following processes:

- Absorption, either by a neutral-density or a color filter, Fig. 1.2a, involves binomial selection of incident photons into transmitted and absorbed photons. If the incident photons are Poisson distributed then both the transmitted and the absorbed photons are also Poisson distributed.
- Beam-splitting or reflection, Fig. 1.2b involves binomial selection of incident photons into transmitted and reflected beams. If the incident photons are Poisson distributed then both the transmitted and the reflected photons are also Poisson distributed.
- Diffraction, Fig. 1.2c, consists of a cascade of binomial selection processes. If the incident photons are Poisson distributed then the photons in each diffracted beam are also Poisson distributed.
- Scattering, Fig. 1.2d, also consists of a cascade of binomial selection processes. If the incident photons are Poisson distributed then the photons observed under any scattering direction are also Poisson distributed.
- Generation of photo-charge pairs in a semiconductor, Fig. 1.2e, involves the interaction of incident photons with the atoms of the solid. If the energy of an incident photon is sufficiently high, the photon can create with a certain probability an electron–hole pair. If the incident photons are Poisson distributed then both the photo-generated charges and the transmitted photons are Poisson distributed.
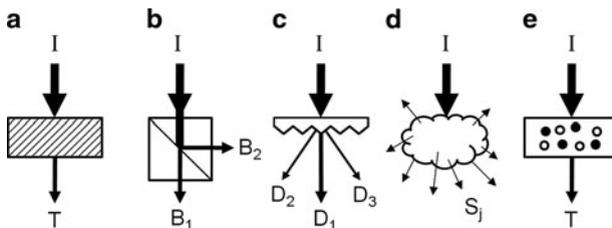

Fig. 1.2 Schematic illustration of the various types of interaction processes occurring between incident electromagnetic radiation I and matter. (**a**) A neutral-density or color filter produces the transmitted reduced intensity T. (**b**) A beam-splitter sends incident photons arbitrarily into one of two beams B_1 and B_2. The intensities B_1 and B_2 can be different. (**c**) A diffraction filter produces several diffracted beams D_j, whose intensities are typically not the same. (**d**) A scattering object produces scattered light S, which can usually be observed in all directions. (**e**) The detection of incident photons with a semiconductor creates charge pairs (photogenerated electrons and holes)

1.5 Noise Properties of Light Sources

In the quantum picture, an electromagnetic wave corresponds to a stream of photons. Depending on the detailed nature of the photon generation process, the statistical distribution of these photons will vary. These statistical properties are summarized later for the four most common light sources employed in practice, coherent light sources such as single-mode lasers, thermal (blackbody radiator) light sources, partially coherent light sources such as discharge lamps and light emitting diodes (LEDs).

1.5.1 Coherent Light (Single-Mode Lasers)

In classical physics, light is described as an electromagnetic wave satisfying Maxwell's equations. In this model, any type of wave in free space can be represented by a linear superposition of plane waves, so-called modes, of the form [6]:

$$U(x, y, z, t) = e^{-i\omega t} e^{i(ux + vy + wz)} \tag{1.3}$$

with the wave vector $\mathbf{k} = (u, v, w)$, the spatial coordinate $\mathbf{r} = (x, y, z)$, time t, and the angular frequency $\omega = |\mathbf{k}|c$. Such a monochromatic beam of light with constant power is called coherent light. The light emitted by a single-mode laser operating well above threshold is a good physical approximation to such a perfectly coherent light source.

Assuming that the emission of photons produced in a coherent light source is the effect of individual, independent emission processes, it can be shown that the emitted number of photons n is a random variable which has a Poisson distribution [2]. As a consequence, the variance s_N of this Poisson distribution is equal to the mean number N of the emitted photons, corresponding to the expectation value $N = <n>$ of n

$$s_N = N. \tag{1.4}$$

1.5.2 Thermal (Incandescent) Light Sources

Light emitted from atoms, molecules, and solids, under condition of thermal equilibrium and in the absence of other external energy sources, is known as thermal light or blackbody radiation. The temperature-dependent spectral energy density of a thermal light source is determined by Planck's blackbody radiation law [6]. If only a single mode of such a blackbody radiation field is considered, the resulting probability distribution of the photon number is not a Poisson but a Bose–Einstein distribution [6], with a variance s_N given by:

$$s_N = N + N^2. \tag{1.5}$$

In practice, it is very rare that only one mode of a blackbody radiation source is of importance, and in most experimental cases the statistical properties of multimode thermal light must be considered. Assuming that a thermal light source contains M independent thermal modes of similar frequencies, it can be shown [7] that the photon number variance s_N of this multimode thermal light source is given by:

$$s_N = N + \frac{N^2}{M}.$$ (1.6)

The number M of thermal modes present in an actual blackbody radiation source is usually very large. When light from a blackbody radiation cavity with volume V is filtered with a narrow-band filter of bandwidth $\Delta\lambda$ around a central wavelength λ, the resulting narrow-band thermal radiation field contains a number M of thermal modes of

$$M = V \frac{8\pi \, \Delta\lambda}{\lambda^4}$$ (1.7)

which follows directly from the mode density in a three-dimensional resonator [6]. As an example, consider an incandescent light source with a cavity volume (filament part) of $V = 1\,\mathrm{mm^3}$, filtered through a narrow-bandwidth filter with $\Delta\lambda = 1\,\mathrm{nm}$ around the central wavelength $\lambda = 600\,\mathrm{nm}$. According to (1.7), this thermal radiation field contains the large number of $M = 1.9 \times 10^8$ thermal modes.

Consequentially, in most practical cases thermal light sources contain such a large number of modes that the statistics of the emitted photon numbers are effectively described by a Poisson distribution. The multimode variance given in (1.6) is then practically equal to the Poisson case (1.4).

As a concluding note, it should be mentioned that even photons from a single thermal mode may approach a Poisson distribution if the detection times are long enough: If the time interval chosen for the individual observations of photon numbers is much larger than the coherence time of the thermal field (the "memory" scale of the field), the photon number statistics are again approaching a Poisson distribution, as has been calculated in detail in [8].

1.5.3 Partially Coherent Light (Discharge Lamps)

The light from a single spectral line of a discharge lamp has classical intensity fluctuations on a time scale determined by the radiation's coherence time τ [2]. This type of light source is, therefore, partially coherent. The intensity fluctuations will give rise to greater fluctuations in photon number than for a source with constant power such as a perfectly coherent source. For this reason, partially coherent light cannot be Poisson distributed. In [7] a semiclassical treatment of the counting statistics of a fluctuating field is given, and it is shown that the variance s_N of the photon number may be expressed as:

$$s_N = N + < \Delta W(t)^2 >,$$ (1.8)

where $W(t)$ denotes the averaged photon count rate during the detection time interval t. If the detection time t is much longer than the coherence time τ then the intensity fluctuations on time-scales comparable to τ will become inconsequential, and the intensity maybe taken as effectively constant. In this case again, the variance of the time-averaged partially coherent light is reduced to the Poisson case (1.4). Typical coherence times of discharge lamps are of the order of 1–100 ns.

1.5.4 Light Emitting Diodes

Semiconductor materials can emit light as a result of electron–hole recombination. A convenient way of achieving this is to inject electrons and holes into the space charge region of a pn-junction by applying a forward bias to it [6]. The resulting recombination radiation is known as injection electroluminescence, and the pn-junction light source is termed LED.

Because of the high conversion efficiency of modern LEDs, the photon statistics of these solid state light sources are strongly influenced by the charge carrier statistics of the injected current. If a stable electronic current source with low internal resistance is employed, the charge carriers in the current I are Poisson distributed, and the variance s_I of the current's so-called shot-noise is given by:

$$s_I = 2\,q\,I\,B, \tag{1.9}$$

where B denotes the bandwidth of the measurement circuit. As a consequence, the photons emitted by the LED are also Poisson distributed, and the variance is given again by (1.4).

It is not difficult, though, to devise a source of current with a sub-Poisson charge carrier distribution. Consider a stable voltage source in series with a resistor R. Because of the thermal coupling of the resistor to its environment with temperature T, the voltage across the resistor's terminals fluctuates statistically with the so-called Johnson noise. The variance s_V of this Johnson noise is given by:

$$s_V = 4kT\,R\,B \tag{1.10}$$

with Boltzmann's constant $k = 1.3807 \times 10^{-23}$ J/K. This voltage noise across a resistor corresponds to a current noise through it, with a variance s_I expressed in terms of the current I and the voltage V across the resistor

$$s_I = \frac{4kT\,I\,B}{V}. \tag{1.11}$$

Comparison of (1.9) and (1.11) reveals that as soon as the voltage across the resistor exceeds a value of $2kT/q$, corresponding to about 52 mV at room temperature, the statistics of the charge carriers in the resistor become sub-Poissonian. Therefore,

instead of driving a high-efficiency LED with a stable current source for the generation of Poisson distributed electroluminescence light, it can be operated with a stable voltage source through a series resistor, resulting in sub-Poissonian statistics of the emitted light [9].

1.6 The Meaning of "Single-Photon Imaging"

In the previous sections we have seen how the statistics of an incident stream of photons are influenced by the various optical and optoelectronic components in the beam path. At the end of this chain, the photons are interacting in an image sensor, where they create electronic charges or charge-pairs; as detailed earlier, these are often Poisson distributed. The final task is electronically to detect and convert these charges into voltage signals, which can then be further processed. Unfortunately, this electronic charge detection is also a statistical process, often with zero mean, as will be discussed in more detail in Sect. 1.9. If the variance of the photons interacting with the image sensor is denoted by s_N and the variance of the electronic photocharge detection process is s_D, the total variance s of the image sensor signal is given by:

$$s = s_N + s_D. \tag{1.12}$$

The consequences of this noisy electronic photocharge detection and process are graphically illustrated in Fig. 1.3 for an image sensor under low-intensity illumination (mean number of interacting photons < 10).

Round symbols in Fig. 1.3 indicate the positions where light sources are imaged onto the image sensor. During the observation time, the light sources may emit a (small) number of photons which then interact with the image sensor (full circles), or no photons interact with the image sensor (open circles), either because
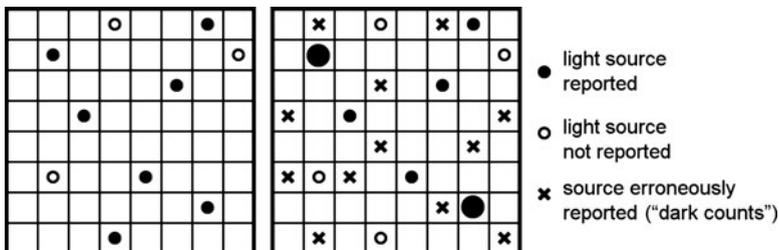

Fig. 1.3 Graphical illustration of the consequences of the noisy electronic charge conversion process taking place in the image sensor and its associated electronics. *Round symbols*: position of light sources. *Full circles*: interaction of photons with the sensor. *Open circles*: no photons detectable. *Crosses*: photons are erroneously reported due to the noise of the electronic charge detection process. *Left*: ideal detection (no electronic noise). *Right*: Real detection (broadened distribution and dark counts)

none are emitted or none are detected by the image sensor. The left-hand picture shows the distribution of photons interacting with the image sensor. The right-hand picture illustrates the effects of the subsequent electronic photocharge detection and conversion process.

The first effect is the broadening of the probability distribution, as seen already in (1.12). As a consequence, the reported number of photons becomes more imprecise, such as interacting photons that may now not be detected any more (previously full circles on the left become open circles on the right); or a number of interacting photons which are reported too high (larger full circles on the right).

The second effect, however, is much more disconcerting in practice: As the electronic noise is acting on all pixels, photons maybe reported even in locations where no light sources are imaged onto the image sensor, so-called "dark counts." This is indicated with crosses on the right-hand picture. If the low-intensity light sources are only sparsely distributed over the image sensor, it can become impossible to identify them if the electronic noise of the charge detection process is too large. Based on this assertion, the following practical definition of the general topic of this book, "single-photon imaging" is proposed:

> Single-photon imaging is the detection of two-dimensional patterns of low-intensity light, i.e. mean photon numbers in the pixels of less than 10, where the electronic photocharge detection process contributes such little noise that the probability of erroneously reporting a photon where there is none is appreciably smaller than the probability of having at least one photon in a pixel.

To determine for each particular case how much variance can be tolerated in the electronic photocharge detection process, it is assumed that the electronic charge detection noise is normally distributed with zero mean and standard deviation σ_D

$$p_D(x) = \frac{1}{\sqrt{2\pi}\,\sigma_D}\ e^{-\frac{x^2}{2\sigma_D^2}}. \tag{1.13}$$

It can be argued that the electronic charge detection process consists of several independent stochastic contributions, and because of the central limit theorem the compound distribution is approaching the Gaussian (1.13) [5]. Note that the output of the image sensor is usually a voltage, but the coordinate x in (1.13) is scaled such that $x = 1$ corresponds to the detection of exactly one photocharge. The probability p of (erroneously) reporting one or more photocharges in a pixel is then given by:

$$p = \int_{0.5}^{\infty} p_D(x)\,\mathrm{d}x = \frac{1}{2}\mathrm{erfc}\left(\frac{1}{\sqrt{8}\,\sigma_D}\right), \tag{1.14}$$

where erfc is the complementary error function, $\mathrm{erfc}(x) = 1 - \mathrm{erf}(x)$ [10]. For a handy estimation of which σ_D is required to reach a given probability p, Winitzki's approximation of the error function $\mathrm{erf}(x)$ is employed, which can easily be inverted algebraically [11]. The following estimate for σ_D results

$$\sigma_D \cong \frac{1}{\sqrt{8}} \sqrt{\frac{2a}{ab - \frac{4}{\pi} + \sqrt{\left(ab - \frac{4}{\pi}\right)^2 + 4ab}}}, \tag{1.15}$$

where $a = 0.147$ and b is the following function of the probability p

$$b = -\ln\left(1 - (1 - 2p)^2\right). \tag{1.16}$$

As an example, if it should be assured that in less than every tenth pixel, $p < 0.1$, a photon is erroneously reported then $\sigma_D < 0.39$ must be achieved. And for $p < 0.01$, $\sigma_D < 0.215$ is necessary.

1.7   Energy Band Model of Solid State Matter

Quantum theory explains the discrete energy levels of the stable states of bound electron-core systems. As a consequence, isolated atoms, ions, and molecules show only discrete energy levels and the interaction with light can only occur if the energy of interacting photons corresponds to a transition between these discrete energy states [4]. In solids, however, the distances between the cores are so small that their bound electrons interact with each other, and the problem must be treated as a many-body system instead of a single electron-core system.

As a consequence, the energy levels of solids are not single lines any more but they are broadened. Since the electrons close to the core are well shielded from the fields of the neighboring cores, the lower energy levels of a solid are not broadened, and they rather correspond to those of the isolated atoms. In contrast, the energies of the higher-lying discrete atomic levels split into closely spaced discrete levels and effectively form bands [6]. This is illustrated in Fig. 1.4a.

The highest partially occupied energy band of a solid is called conduction band, and the energy band just below it is called the valence band. The difference E_g between the highest energy of the valence band E_V and the lowest energy of the conduction band E_C is called the bandgap energy:

$$E_g = E_C - E_V. \tag{1.17}$$

If the conduction band of a solid is partially filled at zero temperature, $T = 0$, the solid is a metal; it conducts current well at any temperature. If, however, the conduction band is completely empty at zero temperature then the solid is a semiconductor; it cannot conduct current at zero temperature because there are no energy states available in the valence band which would correspond to electrons moving freely in the solid. Insulators are just special cases of semiconductors whose bandgap energy E_g is larger than about $5\,\text{eV}$. Actually, solids appearing as "insulators" at moderate temperature are effectively semiconductors at elevated
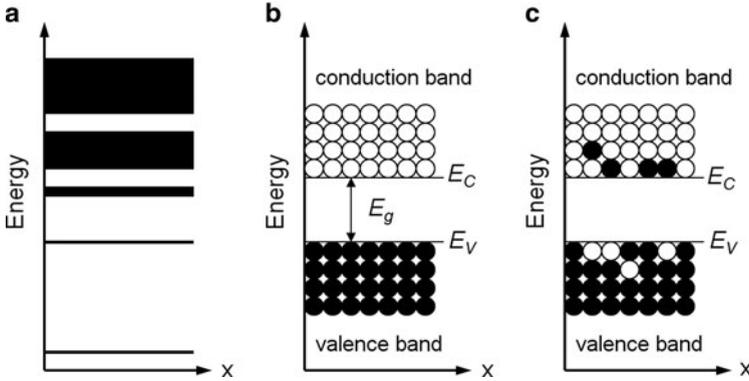
Fig. 1.4 Schematic illustration of the energy distribution of bound electron-core states in solids. (**a**) Broadening of the discrete energy levels of an isolated electron-core system into bands for solid-state material. (**b**) Occupancy of valence and conduction bands in a semiconductor at $T = 0$. (**c**) Occupancy of valence and conduction bands at $T > 0$. *Open circle*: vacant state at this energy level; *filled circle*: occupied state

temperatures. A good example is diamond, with $E_g = 5.45\,\text{eV}$ [13], which is considered to be an insulator at room temperature but diamond is increasingly made use of for the fabrication of semiconductor circuits operating at a high temperatures of $400\,°\text{C}$ and above [14].

1.8 Detection of Electromagnetic Radiation with Semiconductors

The schematic illustration in Fig. 1.4 indicates that the excitation of an electron from the valence band into the conduction band, i.e., the generation of an electron–hole pair, requires an interaction with an energy of at least the bandgap energy E_g. If this interaction energy is provided by an incident photon, which is absorbed in the event, then the created electron–hole pair contributes to the measurement signal. However, if the interaction energy is provided by thermal energy from the environment (a phonon) then the created electron–hole pair contributes to the noise impairing the measurement signal.

1.8.1 Quantum Efficiency and Band Structure

The efficient generation of a photon out of an electron–hole pair requires a semiconductor with a direct bandgap, i.e., the emission process does not require the concurrent presence of an additional phonon, to satisfy the simultaneous conservation of energy and momentum. Fortunately, it is not necessary to fulfill

this requirement for the detection process, because the basic events can occur sequentially: First, an incident photon of sufficient energy excites an electron from the valence band into the conduction band by a so-called vertical transition, i.e., no momentum transfer occurs [8]. It is only afterward that the excited electron moves to the bottom of the conductance band through the fast release of one or several phonons (thermalization), and the created hole moves to the top of the valence band through similar thermalization.

As a consequence, direct- and indirect-bandgap semiconductors are equally efficient in the conversion of incident photons of sufficient energy into electron–hole pairs: Quantum efficiencies of close to 100% can be realized in practice in an intermediate energy range, i.e., almost all incident photons in this energy range will create electron–hole pairs. If the energy of the incident electron is lower than the bandgap energy then the semiconductor is essentially transparent to the incident electromagnetic radiation; if the energy of the incident electron is much larger than the bandgap energy then the incident light is already absorbed in the covering layers of a device, and no or few photons can reach the bulk of the semiconductor and interact there. As a consequence, the photodetection quantum efficiency of a semiconductor drops off toward the infrared and the ultraviolet part of the spectrum.

1.8.2 Thermal Equilibrium and Nonequilibrium Carrier Concentrations

As mentioned earlier, the energy required to create an electron–hole pair can also be provided thermally by the absorption of phonons of sufficient energy from the environment. The higher the temperature, the more phonons are available for the thermal creation of electron–hole pairs. In thermal equilibrium, a pure (undoped) semiconductor has an equal concentration n_i of mobile electrons and holes, the so-called intrinsic carrier concentration, given by:

$$n_i = N_0 \, e^{-\frac{E_g}{2kT}} \propto T^{\frac{3}{2}} \, e^{-\frac{E_g}{2kT}}, \tag{1.18}$$

where the factor N_0 depends only on $T^{3/2}$ and on the effective masses of the electrons in the conduction band and of the holes in the valence band. These values are a function of the exact details of the form of conduction and valence band, and therefore, they are highly specific for each semiconductor. As an example, the intrinsic carrier concentration for silicon, with a bandgap energy of $E_g = 1.12\,\text{eV}$, is $n_i = 1.45 \times 10^{10}\,\text{cm}^{-3}$ at $T = 300\,\text{K}$ [12].

It is very important to note that the foregoing is only true for thermal equilibrium. As the presence of mobile charge carriers in a doped or intrinsic semiconductor in thermal equilibrium makes it impossible to distinguish between this "background" charge and the photogenerated charge, high-sensitivity photosensor devices make all use of fully depleted volumes of semiconductors. In these so-called space charge regions all mobile charge carriers have been removed by an electric field. This is

usually accomplished either with a diode structure (a pn-junction) or an MOS (metal oxide semiconductor) capacitance [12]. In both cases, the background charge is reduced to zero in the depletion region, and the energy distribution of the states looks like Fig. 1.4b, corresponding to the case of zero temperature. As a consequence, the energy distribution of states in the depletion region is *not* in thermal equilibrium, and care must be taken when applying models and equations that only hold true for thermal equilibrium.

1.8.3   Dark Current

As the space charge region of a photodetector is swept clean of all mobile charge carriers, any charge present there must either be a part of the photogenerated signal or it must be thermally produced and belongs to the noise. The thermally produced charge carriers move under the influence of the electric field in the space charge region, resulting in the so-called dark current. This dark current has two components, as illustrated in Fig. 1.5 in the case of an MOS structure.

If the charge carriers are generated within the space charge region, this part of the dark current is called generation current. If charge carriers are thermally generated in the bulk of the semiconductor, it is possible that they move by diffusion to the edge of the space charge region, where they are swept across by the electric field and contribute to the dark current. This part of the dark current is called diffusion current. As indicated in Fig. 1.5, only charge carriers thermally produced at a distance of less than L, the diffusion length, from the space charge region can contribute to the diffusion current.

The generation dark current density j_{gen} in a space charge region of width w, which depends on the voltage V_R with which the photodetector is biased, is calculated according to
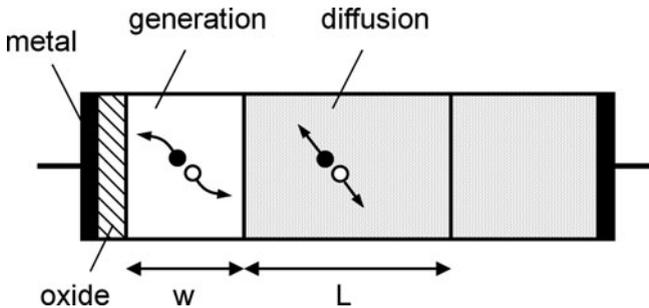

Fig. 1.5 Schematic illustration of the effects contributing to the dark current in an MOS (metal-oxide-semiconductor) structure: Generation current (space charge region width w) and diffusion current (diffusion length L) in the semiconductor

$$j_{\text{gen}} = \frac{q\, n_i}{2\,\tau}\, w(V_R) \tag{1.19}$$

with the generation lifetime τ of electron–hole pairs [12]. In direct bandgap semi-conductors, the lifetime τ is of the order of tens of nanoseconds, and in good-quality indirect bandgap semiconductors, it can be as high as tens of milliseconds [6].

The diffusion dark current density j_{diff} in the bulk of a semiconductor with doping concentration N is given by:

$$j_{\text{diff}} = q\, n_i^2 \frac{D}{NL} \tag{1.20}$$

with the diffusivity D, which is related to the diffusion length L by:

$$L = \sqrt{D\tau}. \tag{1.21}$$

In silicon, it is often the generation current that dominates at room temperature, and the diffusion current becomes important only at elevated temperatures [12]. If only the generation current must be considered, the temperature dependence of the dark current density can be calculated by combining (1.18) and (1.19):

$$j_{\text{dark}} \propto T^{\frac{3}{2}}\, e^{-\frac{E_g}{2kT}}\, w(V_R). \tag{1.22}$$

Modern semiconductor technology makes it possible to reach amazingly low dark current densities, even at room temperature. The lowest value reported to date is $j_{\text{dark}} = 0.15\,\text{pA cm}^{-2}$ at $T = 300\,\text{K}$ in a CCD image sensor [15]. This corresponds to less than one thermally generated electron per second in a pixel of size $10 \times 10\,\mu\text{m}^2$.

1.8.4   Avalanche Effect and Excess Noise Factor

Until now we have always assumed that the number of charge carriers rests constant once created. There is a physical effect, however, which allows to multiply charge packets by arbitrary factors m. This so-called avalanche effect is illustrated in Fig. 1.6. An electron (1) is accelerated in an electric field until it has acquired sufficient energy E_k larger than the bandgap E_g, so that this energy is released in the creation of a secondary electron (2) and a hole (2*). Both electrons are accelerated now until they have acquired sufficient energy for the creation of two pairs of electrons (3) and holes (3*). Of course, the same holds true for the holes, which themselves can create additional electron–hole pairs. This is repeated and leads to a cascade of charge pair creation, effectively multiplying the number N of input charges by a factor m, resulting in a larger charge packet $M = m \times N$. The avalanche multiplication factor m depends strongly on the actual value of the electric field [12].

Fig. 1.6 Schematic
illustration of the avalanche
effect: An electron (1) is
accelerated in an electric field
until it gains sufficient energy
$E_k > E_g$ to create an
electron–hole pair (2) and
(2*). This is repeated and
leads to a cascade of charge
pair creation, effectively
multiplying the input charge
by a field-dependent factor
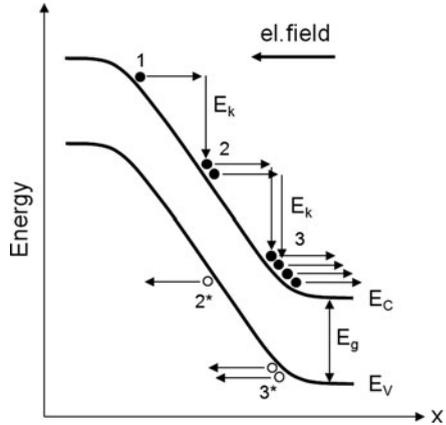
As the avalanche effect is by itself a statistical process, it is not surprising that
avalanche multiplication changes the statistics of the charge packets. If the variance
of the original charge packet is denoted by s_N then the variance s_M of the multiplied
charge packet is given by:

$$s_M = m^2 \, s_N \, F, \tag{1.23}$$

where F denotes the excess noise factor of the avalanche multiplication [5]. Note
that even for completely noise-free multiplication ($F = 1$), the multiplication of a
Poisson input cannot produce a Poisson output: The mean increases linearly with
the multiplication factor, while, according to (1.23), the variance increases with the
square of this factor.

1.9 Electronic Detection of Charge

The last step in the photosensing chain consists of the precise electronic detection of
photogenerated charge packets. Obviously, the electronic charge detection circuits
should add only insignificant amounts of noise, so that also very small charge
packets, down to a single unit charge, can be reliably detected. Although this sounds
like a straightforward, simple task, in reality this is the biggest obstacle today
for solid-state single-photon imaging, apart from the technology-dependent dark
current discussed in Sect. 1.8.3.

The fundamental reason for the fact that electronic circuits and components are
noisy is the interaction of the free electrons with their thermal environment. In the
conducting materials, which are used for the construction of electronic elements, the
motion of the electrons has a random component, because of their nonzero kinetic
energy. According to the law of equipartition [16] the average kinetic energy E_k of
each free electron is given by:

$$E_k = \frac{3}{2} k \, T. \tag{1.24}$$

The random microscopic motion of the free electrons, also called diffusion, has macroscopic electrical effects in the electronic components usually employed for the realization of electronic circuits.

1.9.1 Basic Components of Electronics and their Noise Properties

The three basic components of which most electronic circuits are composed are the resistance, the capacitance, and the transistor, as illustrated in Fig. 1.7. As most photosensors are fabricated today with technology related to Complementary Metal Oxide Semiconductor (CMOS) processes, we will assume for the following that the transistors are of the metal-oxide field-effect (MOS-FET) type [12]. Also, the effects of inductance will be ignored, because they are usually negligible in circuits employed for low-noise electronic charge detection.

In a resistor, illustrated in Fig. 1.7a, diffusion of free electrons results in a random current contribution with zero mean through the device, which in turn causes a fluctuating voltage with zero mean across the resistor's terminals. The variance s_V of the noise voltage and the variance s_I of the noise current, the so-called Johnson noise, as already introduced in (1.10), are given by:

$$s_V = 4kT\,BR; \quad s_I = \frac{4\,kT\,B}{R}, \tag{1.25}$$

where B denotes the bandwidth of the measuring circuit [17]. Note that, the Johnson noise described by (1.25) is only an approximation. The resistor noise is only white (frequency-independent) if the measurement frequencies are below kT/h, corresponding to about 6 THz at room temperature. The quantum mechanically correct spectral noise density distribution shows a drop-off at high frequencies, which is required for a finite total energy contained in the noise [17].

In an ideal capacitance, schematically illustrated in Fig. 1.7b, every "stored" electron on one electrode is compensated by a positive mirror charge on the other electrode, so that charge neutrality is observed. Although, it is not possible to localize such a charge pair on a capacitance, the total number of charge pairs is constant, and, as a consequence, no current noise is created in an ideal capacitance.
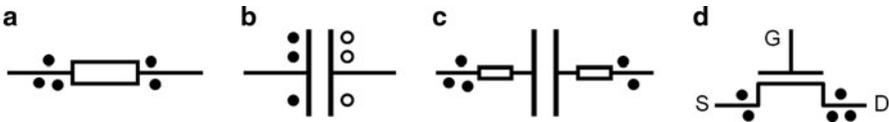

Fig. 1.7 Schematic illustration of the three basic components of electronic circuits, realized with CMOS processes. (**a**) Resistance, (**b**) Ideal capacitance, (**c**) Capacitance with resistive leads, (**d**) Tranistor of the MOS-FET type

However, the leads of a capacitance are not perfect conductors but they are rather resistors, as schematically illustrated in Fig. 1.7c. As described earlier, these resistors are a source of Johnson noise, and this noise spectrum is filtered by the low-pass filter represented by the RC circuit. As the effective bandwidth B of an RC filter is of the order of $1/(R \times C)$, it is immediately concluded from (1.25) that the voltage noise variance s_{Vcap} across a capacitance is proportional to kT/C, and therefore independent of the actual resistance value R. Detailed calculation (integration of the spectral noise density with the appropriate filter function of the RC low-pass filter) yields the following voltage noise variance, also called kTC noise:

$$s_{Vcap} = \frac{kT}{C}.$$ (1.26)

The third key component in an electronic circuit is the transistor. As the predominant semiconductor technology today for the implementation of image sensors is of the CMOS type, the employed transistors are field-effect transistors (FETs). Such a FET is schematically illustrated in Fig. 1.7d, and it consists of a gate electrode G whose voltage V_G is modulating the current I_{DS} flowing from drain D to source S. If the drain–source voltage V_{DS} is not too large then the FET is operating in its linear region as a programmable resistance, for which

$$I_{DS} = 2K(V_G - V_T)V_{DS}.$$ (1.27)

With the geometry- and material-dependent device constant K and the threshold voltage V_T, see for example [18]. The value of the drain–source resistance R_{DS} is therefore given by:

$$R_{DS} = \frac{1}{2K(V_G - V_T)}.$$ (1.28)

As a consequence of the existence of this resistance, the drain–source region of a FET in its linear region exhibits Johnson noise with a variance s_{IDS} given by (1.25):

$$s_{IDS} = \frac{4kTB}{R_{DS}}.$$ (1.29)

This implies that the current across the FET's drain–source terminals is fluctuating statistically, even when the gate voltage is kept absolutely stable.

If the drain–source voltage is large, the FET is operating in its saturation region, and it effectively behaves as a programmable current source [18], where the drain–source current I_{DS} depends quadratically on the gate voltage V_G

$$I_{DS} = K(V_G - V_T)^2.$$ (1.30)

A simple model of the noise properties of a FET in saturation can be derived by assuming that the source–drain region of a transistor consists of two parts: A conducting channel with tapered shape extends from the source toward the

drain region, and it disappears (it "pinches off") close to the FET's drain. The short section between the pinch-off point and the drain consists of a completely depleted semiconductor region. The drain–source current is due to charge carriers that flow down the conducting channel and are injected at the pinch-off point into the depletion region near the drain.

As there are no free charge carriers in a depletion region, the noise properties of a FET in saturation are described by the Johnson noise generated in the conducting channel. Its resistance is approximated by the resistance R_{DS} of the FET in its linear region, as given by (1.28), and the current noise of a FET in its saturation region is consequentially that of a resistance with this value.

Although the physical origin of the current noise of a FET in saturation is the Johnson noise created in the conducting channel, an alternate useful model for the FET's noise performance assumes that the drain–source region is noise-free and that a hypothetical voltage noise source exists at the gate of the FET; this is the so-called "input-referred" voltage noise with variance s_{VG}. It can be estimated using the transconductance g_m, i.e., the differential change of the drain–source current with gate voltage at constant drain–source voltage

$$g_m = \left. \frac{\partial I_{DS}}{\partial V_G} \right|_{V_{DS}=\text{const}} = 2K(V_G - V_T) = \frac{1}{R_{DS}}, \tag{1.31}$$

where use has been made of (1.28) and (1.30). The variance s_{VG} can now be calculated with (1.29) and (1.31):

$$s_{VG} = \left(\frac{\partial I_{DS}}{\partial V_G} \right)^{-2} s_{IDS} = \frac{s_{IDS}}{g_m^2} = \frac{4kTB}{g_m}. \tag{1.32}$$

As mentioned, this is a simplified model for the input-referred channel noise in a FET. A more detailed calculation results in the well-known Klaassen-Prins equation for the input-referred channel noise variance in MOS transistors [19]:

$$s_{VG} = \frac{4kT\,B\,\alpha}{g_m}. \tag{1.33}$$

With a parameter α that depends on the operation regime of the FET. In saturation $\alpha = 2/3$ [19].

As a numerical example, consider a MOS-FET in saturation with a transconductance g_m of $1/g_m = 1\,\text{k}\Omega$, operating at $T = 300\,\text{K}$ and measurement bandwidth $B = 20\,\text{MHz}$. The input-referred root-mean-square voltage noise σ_{VG}, calculated as the square root of the variance s_{VG} in (1.33), is $\sigma_{VG} = 14.86\,\mu\text{V}$.

The statistical variation of the drain–source current in a MOS-FET's channel is only well described by Johnson noise for high frequencies, as illustrated in Fig. 1.8, where the current noise spectral density $S_I(f)$ is shown schematically as a function of temporal frequency f. At lower frequencies, $S_I(f)$ is proportional to $1/f^\beta$, where β is a parameter close to 1 in a wide frequency range [20]. For this reason, the

Fig. 1.8 Schematic
illustration of the current
noise spectral density $S_I(f)$
in a MOS-FET. At lower
frequencies, $1/f$ noise
dominates, while the noise
spectrum is white at higher
frequencies, due to its origin
as Johnson noise in the FET's
channel
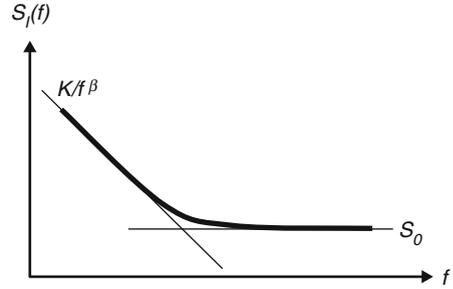
low-frequency part of $S_I(f)$ is called "1/f noise." Typical transition frequencies from 1/f to Johnson noise are between 10 and a few 100 kHz in CMOS transistors.

It is recognized today that the physical origin of 1/f noise in MOS-FETs is the capture and emission of charge carriers from the transistor's channel by traps in the SiO_2 gate oxide [20]. This trapping–detrapping effect causes discrete modulations of the transistor's source–drain conductance called random telegraph signals (RTS) [21]. The superposition of even few RTS already leads to 1/f noise in ordinary MOS-FETs. It should be noted, though, that in deep submicron MOS-FETs, RTS becomes apparent because of the involvement of only a very small number of oxide traps.

1.9.2 Basic Circuits for Electronic Charge Detection

The most common approach to the sensitive electronic detection of charge is to place this charge on the gate of a transistor and to exploit the corresponding change in the transistor channel's electrical properties. In practice, widespread use is made of the source-follower configuration illustrated in Fig. 1.9a, because it combines high dynamic range, excellent sensitivity, and good linearity, while requiring only a small silicon floor space.

Most often, the measurement transistor is loaded with a current source, realized with a MOS-FET in saturation biased with an appropriate voltage V_L [21]. The output voltage V_{SF} then tracks the input voltage V_{in} with good fidelity according to

$$V_{SF} = V_{in} - V_T, \tag{1.34}$$

where V_T denotes the threshold voltage of the measurement MOS-FET.

An alternate circuit for the measurement of small amounts of charge is shown in Fig. 1.9b. This current-sink inverter, also called common-source amplifier, consists of an n-MOS load and a p-MOS measurement transistor, both operating in saturation [21]. It has the advantage over the much more popular source follower in Fig. 1.9a that the small-signal behavior shows voltage amplification, $\Delta V_{inv} = A \times \Delta V_{in}$, with an amplification factor A of the order of 10 [21]. This reduces the noise contribution of the downstream circuits, albeit at the cost of reduced dynamic range [22]. As in
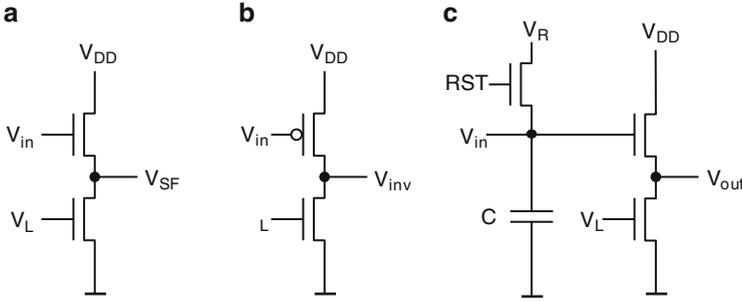
Fig. 1.9 Basic circuits for the electronic detection of charge. (**a**) Source follower with load transistor, (**b**) Current-sink inverter, (**c**) Source follower with reset transistor RST and effective input capacitance C

both cases, the measurement transistor is operating in saturation, the noise properties are comparable, and the white-noise part is adequately described by the Klaassen-Prins equation (1.33).

A more complete pixel circuit, based on a source follower for the detection of photogenerated charge Q on the gate of the measurement transistor, is illustrated in Fig. 1.9c, including a reset transistor (with reset signal RST) and the effective capacitance C at the gate of the measurement MOS-FET. The load transistor can be designed such that its noise contribution is negligible compared to the noise of the measurement transistor. The overall charge measurement noise in Fig. 1.9c is then dominated by the noise of the reset transistor, the so-called reset noise. Using correlated multiple sampling techniques, as described for example in [23], this reset noise is effectively eliminated, and due to the high-pass nature of this filtering, the 1/f part of the noise spectral density is also removed. The remaining noise is white and well described by the Klaassen-Prins equation (1.33). Therefore and as $V_{in} = C/Q$, the root-mean-square noise σ_Q of the charge measurement process is given by:

$$\sigma_Q = C \sqrt{\frac{4kT\,B\,\alpha}{g_m}}. \tag{1.35}$$

As a numerical example for the noise limitations of electronic charge measurement using this source-follower based detection approach, we assume an effective input capacitance C of 50 fF and the same figures as above ($1/g_m = 1\,\mathrm{k\Omega}$, $T = 300\,\mathrm{K}$, $B = 20\,\mathrm{MHz}$). This results in a Johnson-noise limited charge measurement resolution of $\sigma_Q = 4.6$ electrons.

1.9.3 Conclusions for Single-Electron Charge Detection

As explained in Sect. 1.6, the notion of "single-photon electronic imaging" implies that a photocharge detection noise σ_Q of 0.2–0.4 is required, depending on the

actual application. However, as estimated earlier based on (1.35), good solid-state image sensors operating at video frame rates and room temperature achieve typical photocharge detection noise levels σ_Q of 5–10 electrons. It is concluded that an improvement of more than a factor of 10 in the charge detection noise is required. Over the past 20 years, many approaches have been proposed to attain this, and the most important ones are described in this book.

As the dominant noise source in the electronic detection of photocharge is the reset noise in (1.26), it is of foremost importance to reduce or remove it. Fortunately, the correlated multiple sampling (CMS) techniques described in [23] are capable of eliminating reset noise practically completely. Viable circuits for implementing these CMS techniques are presented in Chap. 9 of this book.

As the CMS techniques represent efficient low-pass filters, another important source of noise is eliminated at the same time, the 1/f noise illustrated in Fig. 1.8. It is essential, though, that the measurement band is well above the transition frequency from 1/f noise to Johnson noise, implying that the measurement frequency should not be lower than the typical MOS-FET transition frequencies of 10 to a few 100 kHz.

The remaining source of noise is, therefore, Johnson noise in the channel of the MOS-FET employed for the electronic detection of photocharge, which is at the heart of the charge noise formula (1.35).

The most effectual way to reduce the photodetection charge noise is to lower the effective detection capacitance C. An obvious possibility is to employ minimum-size transistors in deep-submicron semiconductor processes, and this has led to capacitances C of only a few fF. Even smaller values of C can be achieved with special transistor types such as double-gate MOS-FETs or charge-modulating devices (CMDs), as described in Chap. 10 of this book. Capacitances of < 1 fF and single-electron detection noise have been obtained in this way.

Another possibility is to reduce the operation temperature. This is not very effective, however, because the absolute temperature appears under the square root of (1.35). The real benefit of lowering the temperature is reduction of the dark current (1.22) and associated noise, as described in Chap. 2 of this book.

Although it is feasible, in principle, to increase the transconductance g_m in (1.35) by modifying the geometry of the detection MOS-FET, increasing g_m implies increasing the gate capacitance of the transistor, and this more than offsets all improvements achievable in this way.

Finally, reduction of the measurement bandwidth B is a practical and highly successful approach to single-electron photocharge detection, as detailed in Chap. 8 of this book. Although, it is true that reducing the output bandwidth of a conventional image sensor such as a CCD will necessarily decrease also the imager's frame-rate; it is possible to adapt the architecture of the image sensor to resolve this problem. One possibility is to provide the image sensor with a multitude of output channels, and each is operated at reduced bandwidth. A more effective way, which is particularly practical with CMOS image sensors, is to reduce the effective bandwidth of each column without compromising the overall frame rate. It is in this fashion that the subelectron readout results described in [22] or in Chap. 8 have been

obtained. Then again, one might think of intrapixel bandwidth reduction techniques but it appears today that this would not bring much improvement over the column-wise band-pass filtering approaches.

Because of the practical difficulties of achieving subelectron electronic detection noise, a successful alternative is to employ physical amplification mechanisms for the production of more than one charge per interacting photon. A good example of this approach is the employment of the avalanche effect described in Sect. 1.8.4. The advantage of this approach is that it can be integrated monolithically on the same chip and even in each pixel, in particular for the realization of monolithic SPAD imagers, single-photon avalanche photodetectors detailed in Chap. 7 of this book.

There exist also a significant number of alternate approaches making use of physical multiplication effects of photocharge. The most important of these techniques are described in Chaps. 3–6 and 12 of this book.

1.10 Summary: Physical Limits of the Detection of Light

The deliberations of this introductory chapter leave no doubt about the fact that not only does there already exist a multitude of effective single-photon imaging solutions but also more and more monolithic techniques are being developed with a performance approaching that of existing hybrid solutions. As a consequence, single-photon image sensors at lower cost and with enhanced performance are becoming increasingly available, opening single-photon electronic imaging to many more technical applications and even to the consumer market. For this reason, it is interesting to consider what the physical limits are of the detection of light with single-photon resolution.

1.10.1 Sensitive Wavelength Range

As long as the energy of an incident photon is in a range allowing the photon to interact with the detector material, mobile charges are being generated which can subsequently be detected with an electronic charge detection circuit. For high-energy photons (ultraviolet or X-ray region), more than one unit charge is mobilized per photon, and single-photon detection is easy to accomplish, as explained in Chap. 11. If the energy is too high then the detector becomes effectively transparent to the incident radiation. If, on the other hand, the energy of an incident photon is too small – lower than the bandgap in a semiconductor – then the detector also becomes transparent. As an example, silicon is an efficient detector material for single-photon imaging for the wavelength range between 0.1 nm ($E = 12.4$ keV) and 1,000 nm ($E = 1.24$ eV).

If a detector material is employed requiring less energy E_g for the creation of mobile charges – for example a semiconductor with smaller bandgap – then infrared

radiation with longer wavelength can be detected. However, as the dark current increases exponentially with the energy $E_g = hc/\lambda_g$ as described by (1.22), single-photon detection is severely hampered for lower E_g. As an example, the exponential factor in the dark current formula (1.22) is 7,300 times larger for germanium ($\lambda_g = 1,560$ nm) than for silicon ($\lambda_g = 1,120$ nm).

It is concluded that uncooled, room-temperature single-photon electronic imaging is restricted to detector materials with λ_g below about 1,300 nm.

1.10.2 Dark Current and Quantum Efficiency

If a detector needs to exhibit high quantum efficiency then the active thickness of the detector should be comparable to the interaction depth of the photons. If the energy of the incident photons is approaching E_g then the interaction depth becomes quite large, and the active detector thickness should increase correspondingly. However, (1.22) shows that the dark current density increases with the active detector thickness w.

It is concluded that an increase in quantum efficiency is only possible at the expense of increased dark current, and this trade-off is particularly difficult to make if the energy of the incident photons is close to E_g.

1.10.3 Electronic Charge Detection

A key finding of this chapter is the fact that room-temperature electronic detection of charge packets with a resolution of better than one electron r.m.s. is clearly practicable. If this readout noise is less than about 0.2–0.4 electrons r.m.s. one can truly speak of single-electron charge detection.

A combination of such a single-electron charge detection circuit with a suitable photodetector material offering a quantum efficiency of close to 100%, a sufficiently low dark current density and a geometrical fill factor close to unity represents a photosensor with single-photon resolution. Several types of such single-photon electronic image sensors realized using hybrid techniques are described in the chapters of this book.

As the ubiquitous silicon technology allows the realization of on-chip and intrapixel charge detection circuits with less than one electron r.m.s. noise and as silicon offers a quantum efficiency close to 100% over the visible and near infrared spectral range, pixel architectures providing for a geometrical fill factor close to 100% would make it possible to fabricate monolithic and, therefore, cost-effective single-photon electronic imagers. The current development of backside-illuminated CMOS-based image sensor technology, as described in Chap. 2, is exactly this missing link for affordable single-photon imagers, opening single-photon electronic image sensing for wide-spread use in many technical applications and even for the consumer market.

References

1. A. Einstein, Über einen die Erzeugung und Verwandlung des Lichts betreffenden heuristischen Gesichtspunkt, Annalen der Physik, **17**, 132 (1905)
2. M. Fox, *Quantum Photonics – An Introduction* (Oxford University Press, New York, 2006)
3. R.P. Feynman, *Quantum Electrodynamics* (Westview Press, Boulder CO, 1998)
4. D.A.B. Miller, *Quantum Mechanics for Scientists and Engineers* (Cambridge University Press, New York, 2008)
5. H.H. Barrett, K.J. Myers, *Foundations of Image Science* (Wiley, New York, 2004)
6. B.E.A. Saleh, M.C. Teich, *Fundamentals of Photonics* (Wiley, New York, 1991)
7. L. Mandel, E. Wolf, *Optical Coherence and Quantum Optics* (Cambridge University Press, New York, 1995)
8. B.E.A. Saleh, *Photoelectron Statistics* (Springer, Berlin, 1978)
9. F. Wölfl et al., Improved photon-number squeezing in light-emitting diodes, J. Mod. Opt. **45**, 1147 (1998)
10. M. Abramowitz, I.A. Stegun (eds.), *Handbook of Mathematical Functions* (Dover Publications, New York, 1965)
11. S. Winitzki, Uniform approximations for transcendental functions, in *Proceedings of ICCSA-2003, Lecture Notes in Computer Science*, **2667/2003** (Springer, Berlin, 2003), p. 962
12. S.M. Sze, K.K. Ng, *Physics of Semiconductor Devices*, 3rd edn. (Wiley InterScience, New York, 2006)
13. C. Kittel, *Introduction to Solid State Physics*, 8th edn. (Wiley, New York, 2004)
14. E. Kohn, A. Denisenko, Concepts for diamond electronics, Thin Solid Films, **515**, 4333 (2007)
15. E.W. Bogaart et al., Very low dark current CCD image sensor, IEEE Trans. Electr.Dev. **56**, 2642 (2009)
16. F. Reif, *Fundamentals of Statistical and Thermal Physics* (Waveland Press Inc., Long Grove Ill., 2008)
17. H. Nyquist, Thermal agitation of electric charge in conductors, Phys. Rev. **32**, 110 (1928)
18. A.S. Sedra, K.C. Smith, *Microelectronic Circuits*, 6th edn. (Oxford University Press, New York, 2010)
19. F. M. Klaassen, J. Prins, Thermal noise of MOS transistors, Philips Res. Rep. **22**, 505 (1967)
20. C. Jakobson, I. Bloom, Y. Nemirovsky, 1/f noise in CMOS transistors for analog applications from subthreshold to saturation, Solid State Elect. **42**, 1807 (1998)
21. P.E. Allen, D.R. Holberg, *CMOS Analog Circuit Design*, 2nd edn. (Oxford University Press, New York, 2002)
22. Ch. Lotto, P. Seitz, Synchronous and asynchronous detection of ultra-low light levels, in *Proceedings of the 2009 International Image Sensor Workshop*, Bergen, Norway, 26–28 June 2009
23. G.R. Hopkinson, D.H. Lumb, Noise reduction techniques for CCD image sensors, J. Phys. E: Sci. Instrum. **15**, 1214 (1982)

Springer